Turkish Journal of Electrical Engineering & Computer Sciences

http://journals.tubitak.gov.tr/elektrik/

Research Article

Turk J Elec Eng & Comp Sci
(2019) 27: 2881 – 2897
© TÜBİTAK
doi:10.3906/elk-1812-54

# Available transfer capability enhancement with FACTS using hybrid PI-PSO

**Ahmad Abubakar SADIQ**[1,*], **Sunusi Sani ADAMU**[2], **Muhammad BUHARI**[2]
[1]Department of Electrical and Electronics Engineering, School of Electrical Engineering and Technology, Federal University of Technology, Minna, Nigeria
[2]Department of Electrical Engineering, Faculty of Engineering, Bayero University, Kano, Nigeria

**Received:** 11.12.2018 • **Accepted/Published Online:** 05.05.2019 • **Final Version:** 26.07.2019

**Abstract:** In deregulation, growth in electrical loads necessitates improving power delivery, while nondiscriminatory access to transmission grid is a requirement. Deregulation causes a significant rise in transactions, which requires adequate transfer capability to secure economic transactions. In sustainable power delivery, FACTS devices are deployed to enhance available transfer capability (ATC). However, the high investment cost of FACTS makes the problem formulation a multiobjective optimization: power transfer maximization and minimization of FACTS sizes. Furthermore, due to the complexity in optimizing the control variables of voltage source converter types of FACTS, often the solution results in local optima and high computational time. This paper proposes a hybrid of real power flow performance index sensitivity ($\partial PI$) and particle swarm optimization (PI-PSO) to solve the multiobjective optimization of ATC maximization with minimum FACTS sizes using continuation power flow. $\partial PI$ identifies some high-potential locations with enhanced ATC at minimum FACTS size to constitute the PSO's reduced search space. As $\partial PI$ may exhibit masking effects, iterative *n-exponent* and Newton's divided difference approaches are proposed to reduce masking. The proposed PI-PSO is implemented with a thyristor control series compensator and static synchronous series compensator for both bilateral and multilateral transactions. Results show the effectiveness of the proposed PI-PSO over PSO regarding convergence characteristics, avoidance of local optima, and superior ATC values.

**Key words:** Available transfer capability, flexible alternating current transmission systems, performance index, reduced search space, particle swarm optimization

## 1. Introduction

Utilities are embracing deregulated frameworks of supply to ensure sustainable power delivery. A key objective of deregulation is nondiscriminatory access to the transmission grid [1–3]. Bulk transfer of power to load centers is preferred over the grid to ensure economical supply. However, line flows, voltage, and stability constraints hamper the grid's ability to transfer power [4–7]. Consequently, congestion poses a major hindrance to power transfer in a competitive framework characterized by high volume of transactions [8, 9]. Transfer capability enhancement accommodates a high volume of transactions and ensures the power system's security [10]. Based on the definitions and guidelines of the North American Electricity Reliability Council (NERC), total transfer capability (TTC) and available transfer capability (ATC) are used as indexes of transfer capability and hence a measure of transmission grid performance [11]. ATC measures the transfer capability remaining in the grid to accommodate new transactions above already committed uses [12]. To better utilize the transmission grid,

*Correspondence: ahmad.abubakar@futminna.edu.ng



This work is licensed under a Creative Commons Attribution 4.0 International License.

relieve congestion, and enhance transfer capability, FACTS devices are deployed [13, 14]. The FACTS approach uses the power system's parameters as control variables to redistribute power flows [6, 12, 15]. However, due to the high investment cost of FACTS, the problem formulation results in parallel, opposite, and multiobjective optimization: power transfer maximization and minimization of FACTS sizes [3, 16–20].

Power system planning requires the optimization of two or more objectives simultaneously [21]; hence, it is a multiobjective optimization (MOO) formulation. For parallel and opposite objectives, the optimal solution significantly develops into a difficult and complex problem, with local optima likely. In MOO, it is often unclear what constitutes an optimal solution; a solution may be optimal for one objective but local for another [8, 22]. Researchers often adopt classical approaches in tackling MOO: converting the MOO into a single objective (SO) through weighted aggregation, goal programming, and $\varepsilon$-constraints[23]. These methods adopt a compromise solution. However, the compromise is also dependent on the efficiency of the optimization solver [23].

Furthermore, VSC-based FACTS with complex control variables increase the complexity of the MOO problem, which affects the efficiency of the optimization solver [24, 25]. Magnitude and angle of series voltage by static synchronous series compensator (SSSC) varies within $V_{se}^{max} \leq V_{se} \leq V_{se}^{min}$ and $-\pi \leq \delta_{se} \leq \pi$, respectively. In the search space for the SSSC size, each location produces a unique size, as evident in Figure 1. With large population size, improved solutions are at the expense of speed and computational burden. A competitive environment with a high volume of transactions, speed, and accuracy of ATC computations while avoiding local optima is a priority [26]. In this paper, the application of the thyristor control series compensator (TCSC) and SSSC for ATC enhancement of transactions is performed using the proposed hybrid, PI-PSO.

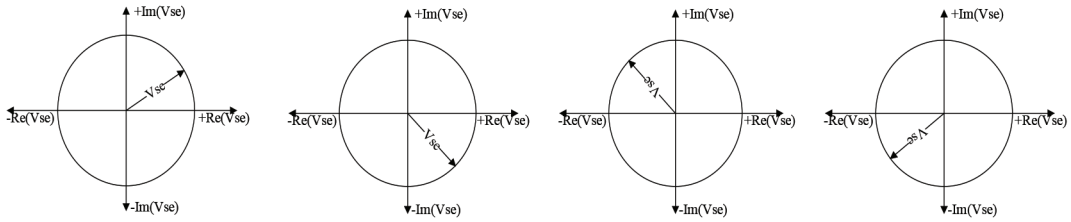


(a) $V_{se}$, $0 \leq \delta_{se} \leq \pi/2$. (b) $V_{se}$, $0 \leq \delta_{se} \leq -\pi/2$ (c) $V_{se}$, $0 \leq \delta_{se} \leq \pi$. (d) $V_{se}$ $0 \leq \delta_{se} \leq -\pi$.

**Figure 1**. Magnitude of series injected voltage by SSSC within the angular search space.

## 2. Static modeling of FACTS using power injection model (PIM)

### 2.1. PIM model of TCSC

Figure 2 depicts the pie model of a transmission line with TCSC ($x_k$). The effective reactance of the line with TCSC is given by Eq. (1), while active and reactive power flows are described by Eqs. (2)–(7).

$$x_{ij}^{new} = x_{ij} - x_k \tag{1}$$

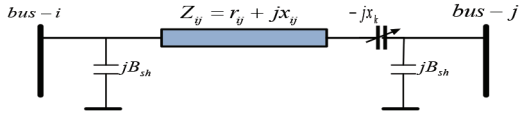


**Figure 2**. Transmission line model with TCSC.

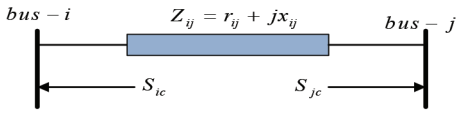


**Figure 3**. Power injection model of TCSC.

$$P_{ij} = V_i^2 G_{ij}^{'} - V_i V_j \left( G_{ij}^{'} \cos\delta_{ij} + B_{ij}^{'} \sin\delta_{ij} \right) \tag{2}$$

$$Q_{ij} = -V_i^2 (B_{ij}^{'} + B_{sh}) - V_i V_j \left( G_{ij}^{'} \sin\delta_{ij} - B_{ij}^{'} \cos\delta_{ij} \right) \tag{3}$$

$$P_{ji} = V_j^2 G_{ij}^{'} - V_j V_i \left( G_{ij}^{'} \cos\delta_{ij} - B_{ij}^{'} \sin\delta_{ij} \right) \tag{4}$$

$$Q_{ji} = -V_j^2 (B_{ij}^{'} + B_{sh}) + V_j V_i \left( G_{ij}^{'} \sin\delta_{ij} + B_{ij}^{'} \cos\delta_{ij} \right) \tag{5}$$

$$G_{ij}^{'} = \frac{r_{ij}}{r_{ij}^2 + (x_{ij} - x_k)^2} \tag{6}$$

$$B_{ij}^{'} = \frac{-(x_{ij} - x_c)}{r_{ij}^2 + (x_{ij} - x_k)^2} \tag{7}$$

Using the PIM, the TCSC is modeled by a line without $jx_k$, with power injections at the terminal buses, as in Figure 3. Eqs. (8)–(11) describe the power injections [7]. Eqs. (12) and (13) give changes in conductance and susceptance, where $\delta_{ij}$ is the voltage angular difference and $\Delta Y_{ij} = \Delta G_{ij} + \Delta B_{ij}$ is line admittance.

$$P_{ic} = V_i^2 \Delta G_{ij} - V_i V_j \left( \Delta G_{ij} \cos\delta_{ij} + \Delta B_{ij} sin\delta_{ij} \right) \tag{8}$$

$$Q_{ic} = -V_i^2 \Delta B_{ij} - V_i V_j \left( \Delta G_{ij} \sin\delta_{ij} - \Delta B_{ij} \cos\delta_{ij} \right) \tag{9}$$

$$P_{jc} = V_j^2 \Delta G_{ij} - V_j V_i \left( \Delta G_{ij} \cos\delta_{ij} - \Delta B_{ij} sin\delta_{ij} \right) \tag{10}$$

$$Q_{jc} = -V_j^2 \Delta B_{ij} + V_j V_i \left( \Delta G_{ij} \cos\delta_{ij} + \Delta B_{ij} sin\delta_{ij} \right) \tag{11}$$

$$\Delta G_{ij} = \frac{x_k r_{ij} \left( x_k - 2x_{ij} \right)}{\left( r_{ij}^2 + x_{ij}^2 \right) \left( r_{ij}^2 + (x_{ij} - x_k)^2 \right)} \tag{12}$$

$$\Delta B_{ij} = \frac{-x_k (r_{ij}^2 - x_{ij}^2 + x_k x_{ij})}{\left( r_{ij}^2 + x_{ij}^2 \right) \left( r_{ij}^2 + (x_{ij} - x_k)^2 \right)} \tag{13}$$

### 2.2. PIM model of SSSC

The SSSC as a VSC-based FACTS compensator inserts a voltage in series with the line through a coupling transformer. The equivalent circuit, modeled by voltage source $V_{se}\angle\delta_{se}$, connected in series with impedance $Z_{se}$ to account for coupling transformer losses, is shown in Figure 4 [27].

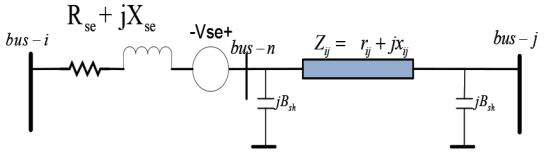


**Figure 4**. Equivalent VSC-based model of SSSC.

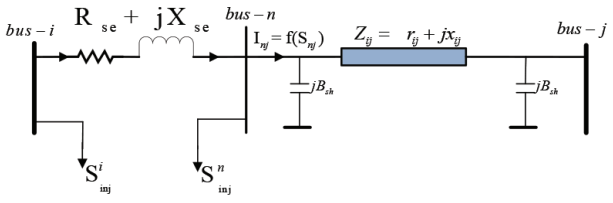


**Figure 5**. Power injection model of SSSC.

Using the Norton equivalent, the series injected voltage by the SSSC is modeled by an equivalent current source in parallel with the coupling transformer impedance [27]. The parallel current expressed by Eq. (14) can be represented by shunt injected current at the SSSC's terminals (bus-i and bus-n) [27]. Since complex nodal power injections are input in load flow calculations, the shunt injected currents of Eqs. (14)-(16) are modeled

by complex loads at buses i and n as shown in Figure 5. Eqs. (17) and (18) give the SSSC's complex power injections [27, 28].

$$I_{inj} = \frac{\overline{V}_{se}}{\overline{Z}_{se}} = \frac{\overline{V}_{se}}{R_{se} + jX_{se}} \tag{14}$$

$$I_{inj} = I_{nj} - I_{in} \tag{15}$$

$$I_{inj} = \left(\frac{P_{nj} + jQ_{nj}}{\overline{V}_n}\right)^* - \left(\frac{\overline{V}_i - \overline{V}_n}{R_{se} + jX_{se}}\right) \tag{16}$$

$$S^i_{inj} = P^{ic}_{inj} + jQ^{ic}_{inj} = \overline{V}_i(I_{inj})^* \tag{17}$$

$$S^n_{inj} = P^n_{inj} + jQ^n_{inj} = -\overline{V}_n(I_{inj})^* \tag{18}$$

In Eqs. (14)–(18), complex bus voltages and impedance are defined as $\overline{V}_i = V_i\angle\delta_i$, $\overline{V}_n = V_n\angle\delta_n$, $\overline{V}_j = V_j\angle\delta_j$, $\overline{V}_{se} = V_{se}\angle\delta_{se}$, and $\overline{Z}_{se} = Z_{se}\angle\delta_{se}$, respectively, while $\overline{Y}_{se} = \frac{1}{\overline{Z}_{se}} = G_{se} + jB_{se}$. Substituting these complex voltages and shunt injected current of Eq. (14) as a function of the admittance $\overline{Y}_{se}$, the real and reactive power injections that model the SSSC are expressed in Eqs. (19)–(22).

$$P^{ic}_{inj} = \mathrm{Re}\left[V_iV_{se}\left(\cos\delta_i + j\sin\delta_i\right)\left(\cos\delta_{se} + j\sin\delta_{se}\right)\left(G_{se} + jB_{se}\right)\right] \tag{19}$$

$$Q^{ic}_{inj} = \mathrm{Im}\left[V_iV_{se}\left(\cos\delta_i + j\sin\delta_i\right)\left(\cos\delta_{se} + j\sin\delta_{se}\right)\left(G_{se} + jB_{se}\right)\right] \tag{20}$$

$$P^{nc}_{inj} = \mathrm{Re}\left[-V_nV_{se}\left(\cos\delta n + j\sin\delta_n\right)\left(\cos\delta_{se} + j\sin\delta_{se}\right)\left(G_{se} + jB_{se}\right)\right] \tag{21}$$

$$Q^{nc}_{inj} = \mathrm{Im}\left[-V_nV_{se}\left(\cos\delta n + j\sin\delta_n\right)\left(\cos\delta_{se} + j\sin\delta_{se}\right)\left(G_{se} + jB_{se}\right)\right] \tag{22}$$

Using the MATLAB symbolic toolbox, the static model of the SSSC is expressed by Eqs. (23)–(26).

$$P^{ic}_{inj} = V_iV_{se}\left[G_{se}\cos(\delta_i - \delta_{se}) + B_{se}\sin(\delta_i - \delta_{se})\right] \tag{23}$$

$$Q^{ic}_{inj} = -V_iV_{se}\left[G_{se}\sin(\delta_i - \delta_{se}) - B_{se}\cos(\delta_i - \delta_{se})\right] \tag{24}$$

$$P^{nc}_{inj} = -V_nV_{se}\left[G_{se}\cos(\delta_n - \delta_{se}) + B_{se}\sin(\delta_n - \delta_{se})\right] \tag{25}$$

$$Q^{nc}_{inj} = V_nV_{se}\left[G_{se}\sin(\delta_n - \delta_{se}) - B_{se}\cos(\delta_n - \delta_{se})\right] \tag{26}$$

## 3. Problem formulation

From the literature, ATC computation methods can be classified as follows: (i) AC/DC power transfer distribution factor (PTDF) [1, 29, 30]; (ii) repeated power flow (RPF) [31, 32]; (iii) optimal power flow (OPF) [33]; and (iv) continuation power flow (CPF) [34, 35].

PTDF relies on sensitivity to power flows, while RPF depends on an arbitrarily chosen step, which is optimistic and computationally tasking. OPF methods, while efficient, involve complex iterative power system optimization, which can result in singularity. CPF introduces a loading parameter $\lambda$ to parameterize and solve the power flow equations to avoid ill-conditioning and singularity [35]. The problem formulation in [12, 32, 35] shows there is a close connection between optimization, CPF, and RPF for ATC computations. Detailed documentation of CPF for ATC computation was reported in [12, 34–36]. Consequently, ATC enhancement with FACTS evaluates an optimization objective as expressed in Eq. (27) using CPF [37], subject to Eqs. (28)–(34).

$$\underset{(\lambda, x_k, V_{se}, \delta_{se})}{Maximize}\left\{ATC = \sum_{\mathrm{i}\in\mathrm{sink}} \mathrm{P}^i_L\left(\lambda_{limited}\right) - \sum_{\mathrm{i}\in\mathrm{sink}} \mathrm{P}^{\mathrm{i}}_{\mathrm{L}}(\lambda = 0)\right\} \tag{27}$$

$$f(x, \lambda) = 0 \tag{28}$$

$$0 \leq \lambda \leq \lambda_{limited} \tag{29}$$

$$P_g^{\min} \leq P_g \leq P_g^{\max} \tag{30}$$

$$Q_g^{\min} \leq Q_g \leq Q_g^{\max} \tag{31}$$

$$S_{ij} \leq S_{ij}^{rated} \tag{32}$$

$$V_i^{\min} \leq V_i \leq V_i^{\max} \tag{33}$$

$$X_{FACTS}^{\min} \leq X_{FACTS} \leq X_{FACTS}^{\max} \tag{34}$$

Eq. (28) is the compact power flow equation. State variable $x = (V, \delta)$ is voltage magnitude and angle. In Eqs. (29)–(33), $\lambda_{limited}$, $P_g$, $Q_g$, $S_{ij}$, and $V_i$ are the loading parameter, real, reactive, apparent power flows, and voltage magnitude $i$, respectively. The objective of the minimum FACTS size is treated as a constraint and imposed by Eq. (34). $X_{FACTS}$ is the controllable parameter, $-0.8 \leq X_{TCSC} \leq 0.2$ for TCSC, while the magnitude of $\overline{V}_{se}$ is within $0 \leq V_{se} \leq V_{se}^{max}$ and obtained by Eq. (35). In Eq. (27), since ATC is in MW, sensitivities of MW flows ($\partial PI$) to FACTS control parameters can be obtained. Using $\partial PI$, the candidate locations for enhanced ATC at minimal FACTS sizes constitute the PSO's RSS.

$$V_{se}^{\max} = 0.5 * \left(V_i^{\max} - V_i^{\min}\right) \tag{35}$$

## 4. Formation of reduced search space for FACTS location

Since line overloads are major constraints for ATC [8], the quality of a candidate line to enhance ATC can be evaluated using $\partial PI$ [38]. The second-order real power flow performance indices ($PI_2$), commonly used as a measure of severity of overload [39], are expressed by Eq. (36). Without change in principle, this is applicable for the determination of FACTS location in congestion management [39–43]. Accordingly, when power flow congestion limits the power transfer transaction, Eq. (37), which evaluates $\partial PI_2$ with respect to FACTS control parameters ($X_{FACTS}$), obtains candidate locations of FACTS for ATC enhancement.

$$PI_2 = \sum_{m=1}^{N_L} \frac{w_m}{2n} \left(\frac{P_{lm}}{P_{lm}^{\max}}\right)^{2n} \tag{36}$$

$$\frac{\partial PI_2}{\partial X_{facts}} = \sum_{m=1}^{N_L} w_m P_{lm}^{(2n-1)} \left(\frac{1}{P_{lm}^{\max}}\right)^{2n} \frac{\partial P_{lm}}{\partial X_{facts}} \tag{37}$$

In Eqs. (36) and (37), $N_L$ is the number of lines, $W_m$ is a nonnegative coefficient, $n$ is $n$-*exponent* order, $P_{lm}$ is active flow, and $P_{max}$ is line capacity. Eq. (38) expresses $P_{lm}$ as the sum of real power injections [44].

$$P_{lm} = \begin{cases} \sum_{n=1, n\neq s}^{nb} S_{mn} P_n & for\ m \neq k \\ \sum_{n=1, n=s}^{nb} S_{mn} P_n + P_j & for\ m = k \end{cases} \tag{38}$$

In Eq. (38), $s$ is the slack bus, nb is number of buses, and $S_{mn}$ is the $mn$th element of matrix [**Sf**] that relates line power flows with bus power injections. The partial derivative of the $P_{lm}$ term in Eq. (37), with respect to the FACTS control parameter, is expressed by Eq. (39).

$$\frac{\partial P_{lm}}{\partial X_k} = \begin{cases} \left( S_{mi} \dfrac{\partial P_i}{\partial X_k} + S_{mj} \dfrac{\partial P_j}{\partial X_k} \right) & for\ m \neq k \\ \left( S_{mi} \dfrac{\partial P_i}{\partial X_k} + S_{mj} \dfrac{\partial P_j}{\partial X_k} \right) + \dfrac{\partial P_j}{\partial X_k} & for\ m = k \end{cases} \tag{39}$$

### 4.1. Sensitivity of PI to TCSC's reactance

For TCSC, the derivative terms of Eq. (39) are obtained from Eqs. (8) and (10), the PIM model of the TCSC. Eqs. (40)–(43) express the derivative of power injections with respect to $x_k$ [40].

$$\left.\frac{\partial P_i}{\partial X_k}\right|_{x_k=0} = \left.\frac{\partial P_{ic}}{\partial x_k}\right|_{x_k=0} = (V_i^2 - V_i V_j \cos\delta_{ij}) \left.\frac{\partial \Delta G_{ij}}{\partial X_k}\right|_{x_k=0} - (V_i V_j \sin\delta_{ij}) \left.\frac{\partial \Delta B_{ij}}{\partial X_k}\right|_{x_k=0} \tag{40}$$

$$\left.\frac{\partial P_j}{\partial X_k}\right|_{x_k=0} = \left.\frac{\partial P_{jc}}{\partial x_k}\right|_{x_k=0} = (V_j^2 - V_i V_j \cos\delta_{ij}) \left.\frac{\partial \Delta G_{ij}}{\partial X_k}\right|_{x_k=0} + (V_i V_j \sin\delta_{ij}) \left.\frac{\partial \Delta B_{ij}}{\partial X_k}\right|_{x_k=0} \tag{41}$$

$$\left.\frac{\partial \Delta G_{ij}}{\partial x_k}\right|_{x_k=0} = 2G_{ij}B_{ij} \tag{42}$$

$$\left.\frac{\partial \Delta B_{ij}}{\partial x_k}\right|_{x_k=0} = B_{ij}^2 - G_{ij}^2 \tag{43}$$

### 4.2. Sensitivity of PI to SSSC's series injected voltage

For SSSC, the derivative terms of Eq. (39) are from Eqs. (23)–(25), the PIM model of the SSSC. Eqs. (44) and (45) express the derivative with respect to the magnitude of series voltage by SSSC $V_{se}$.

$$\left.\frac{\partial P_i}{\partial X_k}\right|_{x_k=0} = \left.\frac{\partial P_{inj}^{ic}}{\partial V_{se}}\right|_{V_{se}=0} = V_i \left[G_{se}\cos(\delta_i + \delta_{se}) - B_{se}\sin(\delta_i + \delta_{se})\right] \tag{44}$$

$$\left.\frac{\partial P_j}{\partial X_k}\right|_{x_k=0} = \left.\frac{\partial P_{inj}^{nc}}{\partial V_{se}}\right|_{V_{se}=0} = -V_n \left[G_{se}\cos(\delta_n + \delta_{se}) - B_{se}\sin(\delta_n + \delta_{se})\right] \tag{45}$$

Note that in Eqs. (40)–(45), sensitivities are obtained as $X_{FACTS}$ tends to zero (i.e. $X_{FACTS} \to 0$ ).

### 4.3. Masking effect in PI sensitivities

In FACTS control operations, the rerouting of power flow from a line causes increased loading in other lines; $\partial PI_2$ may indicate these higher loadings as noncritical. Masking is the inability of $\partial PI_2$ to discriminate between several higher loadings and a huge violation [43]. Consequently, sensitivity-based FACTS locations may exhibit masking. Identification of masking in $\partial PI_2$ is achieved by vector norm-based formulation of Eq. (36) and permits a quantitative explanation of masking [44]. Eq. (46) describes the $\partial PI_2$ values.

$$\left.\begin{array}{ll} \partial PI_2 \leq 1 & \text{No limit violation} \\ \partial PI_2 > \sqrt[n]{N_L} & \text{At least a limit violation} \\ 1 < \partial PI_2 \leq \sqrt[n]{N_L} & \text{Masking effect range} \end{array}\right\} \tag{46}$$

### 4.4. Determination of *n-exponent* to cancel out masking

Since masking range decreases with the *n-exponent* from Eq. (46), a higher-order *n-exponent* leads to $\partial PI_n$ free from masking [44, 45]. This paper proposes two approaches to determine *n-exponent* for reduced masking effect.

***Iterative n-exponent*:** In the case where masking effect is detected, $\partial PI_n$ is evaluated iteratively with higher *n-exponent* according to Eq. (47), and a stopping criterion is enforced as described in Eq. (48).

$$n^{i+1} = n^i + 1 \qquad \text{for } 2 \leq n^i \leq 10 \tag{47}$$

$$\left.\begin{aligned} \partial PI_n < 0 \quad \partial PI \text{ changes sign} \\ n^{i+1} \geq 10 \quad 20^{th} \text{ order exponent} \end{aligned}\right\} \tag{48}$$

***Newton's divided difference*:** In addition to computational burden, in a case where the masking effect is a result of multiple lines, the iterative *n-exponent* becomes poor. Accordingly, Newton's difference method estimates $\partial PI_n$ as expressed in Eq. (49), which assumes: (i) a linear variation between $\partial PI_2$ and $\partial PI_{20}$ to compute the *n-exponent* of $\partial PI_n$, and (ii) by approximate techniques, $\partial PI_{20}$ can be estimated as in [44].

$$\partial PI_n = 0.5\partial PI_{20} \tag{49}$$

Therefore, $\partial PI_n$ (with minimal masking) is between $\partial PI_2$ (with masking) and $\partial PI_{20}$ (without masking). Hence, Eqs. (50), (51), and (52) give Newton's divided difference, the interpolation equation, and the definition of terms used in Eqs. (50) and (51), respectively, while the *n-exponent* is as in Eq. (53). The RSS thus constitutes lines with negative $\partial PI_2$ and $\partial PI_n$ as in Eq. (54).

$$\partial PI(n_0, n_1) = \frac{\partial PI_{n_1} - \partial PI_{n_0}}{n_1 - n_0} \tag{50}$$

$$\partial PI_n = \partial PI_{n_0} + (n - n_0)\partial PI(n_0, n_1) \tag{51}$$

$$\left.\begin{aligned} \partial PI_{n_0} &= \partial PI_2 \\ \partial PI_{n_1} &= \partial PI_{20} \\ \partial PI_n &= 0.5\partial PI_{20} \end{aligned}\right\} \tag{52}$$

$$n = \frac{\partial PI_n - \partial PI_{n_0}}{\partial PI(n_0, n_1)} \tag{53}$$

$$\mathbb{N} = [RSS_{\partial PI_2}; RSS_{\partial PI_n}] \tag{54}$$

***Criteria to constitute the RSS*:** Generally, all sensitive lines constitute the RSS, and:

i. All lines with negative sensitivities with respect to the FACTS control parameter constitute the PSO's RSS.

ii. All lines containing generator buses are excluded even if the sensitivity is negative.

## 5. Proposed hybrid performance index and particle swarm optimization (PI-PSO)

To achieve a compromise between speed and accuracy, the PSO's parameters are carefully selected [46, 47]. However, in the proposed PI-PSO, $\partial PI$ enables formation of the RSS, which improves the particle's exploitation by avoiding local optimal solutions. A particle's position is described by Eq. (55), such that $\lambda$ and $\eta$ are location

and size, respectively. For the RSS of m dimensions in Eq. (56), in addition to updates of particles' positions in PSO, position update in PI-PSO is described in Eq. (57). The parameters of PSO are weight($\omega = 0.9$), acceleration factors ($C_1 = 1.5$ and $C_2 = 4 - C_1$ ), iteration ($Max_{It} = 150$), and swarm size($N_L$ = number of lines). Figures 6 and 7 show the flowchart of PI-PSO and a one-line diagram of the test network, which is the IEEE 9-bus system with 3 transformers and 6 transmission lines at 230 kV; total load of the system is 315 MW and 115 MVar [47].

$$X_i^k = [\lambda_i^k, \eta_i^k] \tag{55}$$

$$\mathbb{N} = [\lambda_1, \lambda_2, \cdots \lambda_m] \tag{56}$$

$$X_i^{k+1} = \begin{Bmatrix} X_i^{k+1}(\lambda_i) & if \lambda_i^{k+1} \in \mathbb{N} \\ \mathbb{N}(randperm(m,1)) & if \lambda_i^{k+1} \notin \mathbb{N} \\ X_i^{k+1}(\eta_i) & for\ \eta_i \in \mathbb{R} \end{Bmatrix} \tag{57}$$

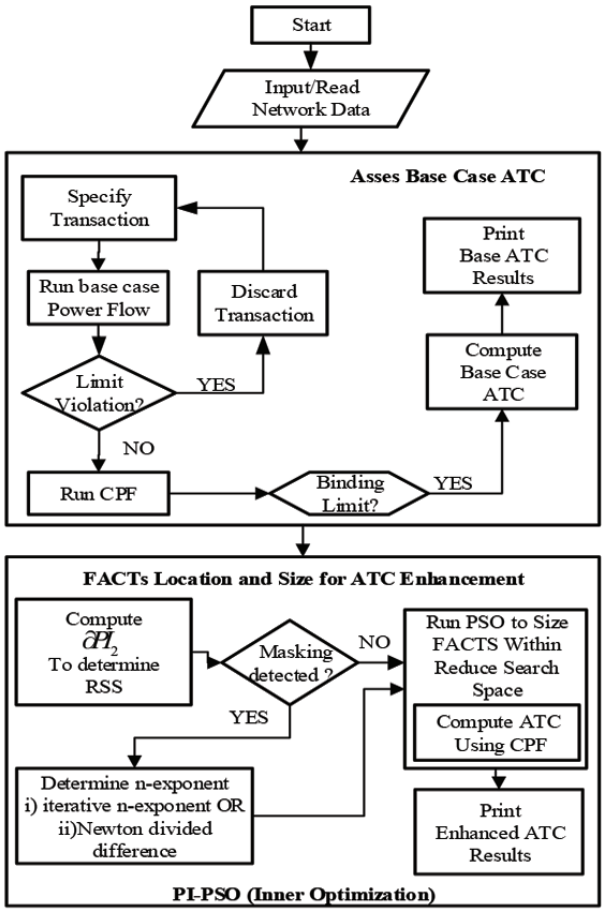


**Figure 6**. Flowchart of hybrid PI-PSO.

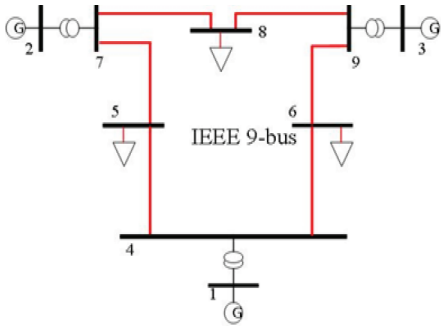


**Figure 7**. One-line diagram of test system.

## 6. Implementation

MATPOWER, a steady-state power system analysis tool [48], implements the proposed methodology. ATC assessment is executed using MATPOWER's CPF. The CPF features were extended to enforce the constraints

of Eqs. (32) and (33). Event detection and callback functions were contributed by MATPOWER on GitHub, acknowledged by the MATPOWER community. Highlights of this paper include the following:

i. Reduction of the entire search space for FACTS location and identification of lines with enhanced ATC at minimal FACTS sizes to constitute the RSS using $\partial PI_n$.
ii. A hybrid PI-PSO for ATC enhancement with improved convergence and efficiency.
iii. Determination of *n-exponent* using an iterative approach and Newton's divided difference method.

## 7. Results and discussion

Transfer directions of some transactions are described in the 2nd and 3rd columns of Table 1. Also, Table 1 and Table 2 show $\partial PI_2$ with TCSC and SSSC. Locations that constitute the RSS are in bold. In Table 1, the most positive $\partial PI_2$ corresponds to the base case limiting line and is due to the capacitive model of the TCSC in $\partial PI_2$.

**Table 1**. Second-order sensitivity ($\partial PI_2$) to TCSC's reactance ($n = 2$).

| Trans. | Source | Sink | Line number (terminating buses) | | | | | | | | |
|---|---|---|---|---|---|---|---|---|---|---|---|
| ID | buses | buses | 1(1 to 4) | 2(4 to 5) | 3(5 to 7) | 4(2 to 7) | 5(7 to 8) | 6(8 to 9) | 7(9 to 3) | 8(9 to 6) | 9(6 to 4) |
| **T1** | 1, 3 | 5 | 0.0137 | **-0.7046** | *1.7751* | 0.0898 | **-0.1183** | 0.6834 | -0.0484 | **-0.9763** | **-0.0192** |
| **T2** | 1, 2 | 5, 8 | -0.0273 | 0.2582 | **-0.5396** | -0.0268 | *0.9141* | **-0.1696** | 0.0368 | 0.4394 | **-0.4586** |
| **T3** | 1, 2,3 | 5, 6 | 0.0772 | 0.0314 | *1.2980* | 0.0765 | **-0.3613** | 0.0104 | -0.0322 | **-0.5668** | 0.3071 |
| **T4** | 1, 2,3 | 6, 8 | -0.0696 | **-0.1910** | **-0.4354** | -0.0201 | *0.8763* | **-0.1804** | 0.098 | 0.8005 | **-0.6959** |
| **T5** | 2, 3 | 5 | 0.0437 | 0.0677 | *1.4802* | 0.0726 | **-0.4457** | 0.0698 | -0.0204 | **-0.6223** | 0.0711 |
| **T6** | 1 | 8 | -0.0586 | 0.7089 | **-0.1627** | 0.0104 | *1.1636* | **-1.0226** | -0.006 | 0.0126 | **-1.5384** |
| **T7** | 1, 2, 3 | 5, 8 | 0.0327 | 0.022 | *0.7473* | 0.0623 | **-0.0046** | 0.0209 | 0.0113 | **-0.0078** | 0.0048 |
| **T8** | 2, 3 | 6 | 0.0600 | 0.1719 | *1.103* | 0.0663 | **-0.2554** | **-0.0135** | -0.0235 | **-0.4267** | 0.198 |
| **T9** | 1, 2 | 8 | -0.0343 | **-0.1271** | **-0.6524** | -0.0193 | *1.1083* | **-0.143** | 0.0375 | 0.5739 | **-0.4826** |
| **T10** | 1, 2 | 5, 6 | 0.0465 | 0.0258 | *0.6759* | 0.0413 | **-0.0116** | 0.0021 | 0.0086 | **-0.0414** | **-0.007** |

**Table 2**. Second-order sensitivity ($\partial PI_2$) to SSSC's series injected voltage ($n = 2$).

| Trans. | Line number (terminating buses) | | | | | | | | |
|---|---|---|---|---|---|---|---|---|---|
| ID | 1(1 to 4) | 2(4 to 5) | 3(5 to 7) | 4(2 to 7) | 5(7 to 8) | 6(8 to 9) | 7(9 to 3) | 8(9 to 6) | 9(6 to 4) |
| **T1** | -0.0570 | 3.4411 | **-5.3290** | 0.5169 | 0.4379 | **-3.3775** | -0.2709 | 5.1170 | 0.0364 |
| **T2** | -0.0841 | **-1.0880** | 4.6866 | 2.2759 | **-3.5912** | 0.9938 | -0.0970 | **-1.9424** | 2.5540 |
| **T3** | -0.2885 | **-0.0964** | **-2.6338** | 1.6763 | 2.5468 | **-0.1333** | -0.0142 | 3.3301 | **-1.3878** |
| **T4** | 0.2544 | 1.0153 | 4.4098 | 2.4144 | **-3.2473** | 1.0180 | -0.3463 | **-3.5896** | 3.9137 |
| **T5** | -0.1436 | **-0.2564** | **-3.6751** | 1.4946 | 2.8103 | **-0.4357** | -0.0756 | 3.4646 | **-0.3659** |
| **T6** | 0.1269 | **-3.1581** | 1.3391 | 0.0615 | **-6.7268** | 5.5265 | 0.4957 | 0.3898 | 8.0399 |
| **T7** | -0.1154 | **-0.0411** | 0.4360 | 2.4735 | 1.2911 | **-0.0552** | -0.1271 | 0.3864 | 0.0022 |
| **T8** | -0.2220 | **-0.6847** | **-1.6413** | 1.8837 | 2.2394 | 0.0266 | -0.0811 | 2.887 | **-0.8476** |
| **T9** | 0.0842 | 0.7067 | 4.6791 | 1.9622 | **-4.5912** | 0.8256 | -0.1232 | **-2.5717** | 2.6148 |
| **T10** | -0.1783 | **-0.0532** | 0.7081 | 2.4452 | 1.102 | **-0.0309** | -0.0141 | 0.3635 | 0.557 |

From Table 2, based on established criteria of RSS and Eq. (46), $\partial PI_2$ of **T7** and **T10** exhibit masking. Consequently, Figures 8a and 8b depict surface plot of $\partial PI_n$ for n-exponents up to 10.

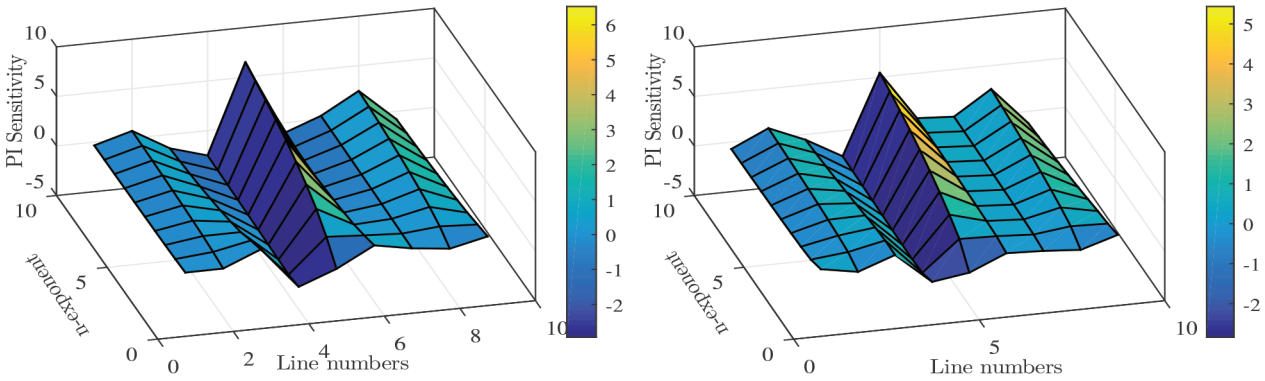


(a) Surface plot of $\partial PI_2$ with respect to $V_{se}$ for **T7**. (b) Surface plot of $\partial PI_2$ with respect to $V_{se}$ for **T10**.

**Figure 8**. Surface plot of sensitivities with respect to SSSC's series injected voltage.

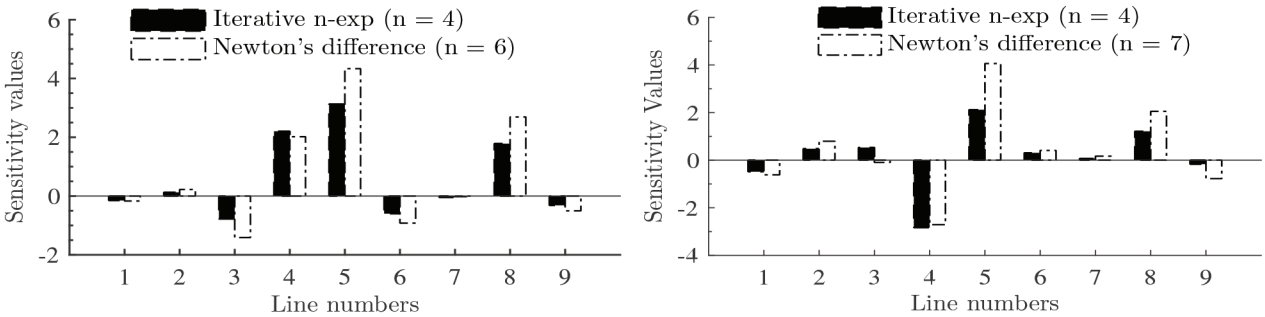


(a) Transaction **T7**. (b) Transaction **T10**.

**Figure 9**. Comparison of masking reduction methods.

$\partial PI_n$ of lines 3, 6, and 9 for **T7** as well as 3 and 9 for **T10** decrease and become negative as the n-exponent increases. The proposed methods in Section 4.4 evaluate $\partial PI_n$ with higher n-exponents. Figures 9a and 9b compare sensitivities for **T7** and **T10**, respectively. From Figure 9 and Table 2, the RSS for **T7** and **T10** constitutes lines 2, 3, 6, and 9. The iterative method requires more computational time and is less effective to handle masking at multiple lines.

To demonstrate the effectiveness of the proposed PI-PSO, an exhaustive search with discrete sizes for **T2** and **T3** is shown in Figures 10a and 10b, respectively.

In Figure 10a, lines 3, 6, and 9 enhance ATC with discrete TCSC sizes, consistent with $\partial PI_2$ in Table 2. ATC increases in line 3 and peaks at 153.4692 MW with 40% and 149.8539 MW with 50% TCSC size; this suggests an optimal ATC in line 3 between 40% and 50%. Similarly, in Figure 10b, lines 2, 3, 6, and 9 record enhancement with discrete $V_{se}$, consistent with the RSS of Table 3. ATC values are 143.0192 MW with 0. 05 p.u. and 142.8792 MW at 0. 06 p.u. in line 3, suggesting optimal ATC in line 3 between 0.05 p.u. and 0.06 p.u. Table 3 and Table 4 give ATC using both PSO and PI-PSO with TCSC and SSSC, respectively. From Table 3, although ATC by PI-PSO is slightly higher in some transactions, PSO produces similar ATC values, attributable to the noncomplex nature of the TCSC's control parameter.

Figures 11a–11d illustrate convergence curves for a typical run of PSO and PI-PSO with TCSC; the RSS improves the random starting point of PI-PSO compared to PSO.

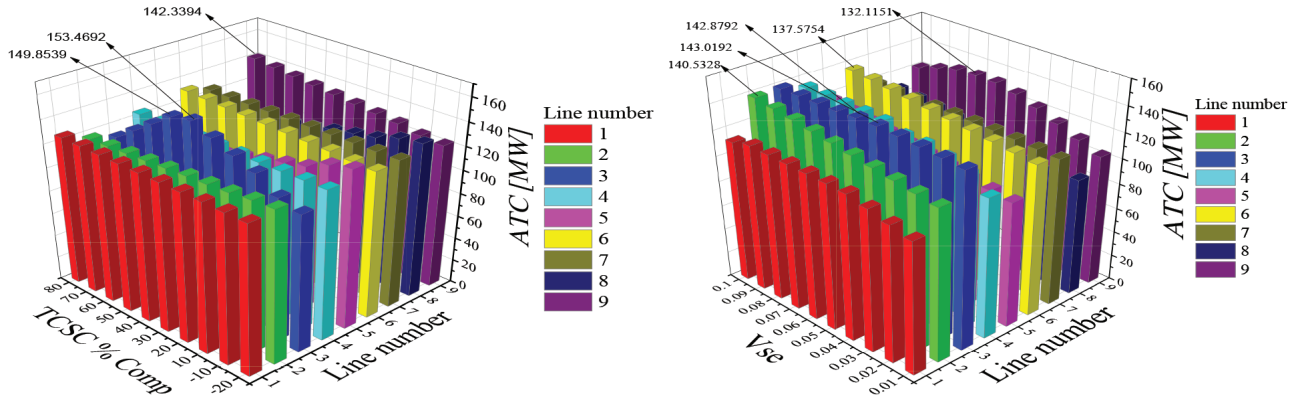


(a) Variation of ATC with TCSC's % Comp. for **T2**. (b) Variation of ATC with SSSC's $V_{se}$ for **T3**.

**Figure 10**. Exhaustive search for ATC enhancement at all locations with TCSC and SSSC.

**Table 3**. ATC values with TCSC using PSO and PI-PSO.

| Trans. | ATC [MW] | | | PSO solution | | PI-PSO Solution | |
|---|---|---|---|---|---|---|---|
| ID | Base case | PSO | PI-PSO | Line no. | %Comp | Line no. | %Comp |
| **T1** | 143.2545 | 182.0445 | 182.0445 | 8(9 to 6) | 80.0000 | 8(9 to 6) | 80.0000 |
| **T2** | 127.1567 | 153.8496 | 153.8509 | 3(5 to 7) | 46.6020 | 3(5 to 7) | 46.6243 |
| **T3** | 118.0243 | 172.6364 | 172.6368 | 8(9 to 6) | 75.9992 | 8(9 to 6) | 76.0102 |
| **T4** | 155.1414 | 181.0710 | 181.0729 | 3(5 to 7) | 38.9338 | 3(5 to 7) | 38.9587 |
| **T5** | 43.6314 | 64.4040 | 64.4040 | 8(9 to 6) | 80.0000 | 8(9 to 6) | 80.0000 |
| **T6** | 128.0228 | 158.7672 | 158.7672 | 9(6 to 4) | 80.0000 | 9(6 to 4) | 80.0000 |
| **T7** | 138.6407 | 151.8797 | 151.8813 | 5(7 to 8) | 57.1509 | 5(7 to 8) | 57.2176 |
| **T8** | 74.6104 | 101.5460 | 101.5460 | 8(9 to 6) | 57.3975 | 8(9 to 6) | 57.3979 |
| **T9** | 60.2851 | 79.5976 | 79.5977 | 3(5 to 7) | 65.3652 | 3(5 to 7) | 65.3655 |
| **T10** | 159.4606 | 172.0520 | 172.0521 | 8(9 to 6) | 35.0626 | 8(9 to 6) | 35.0626 |

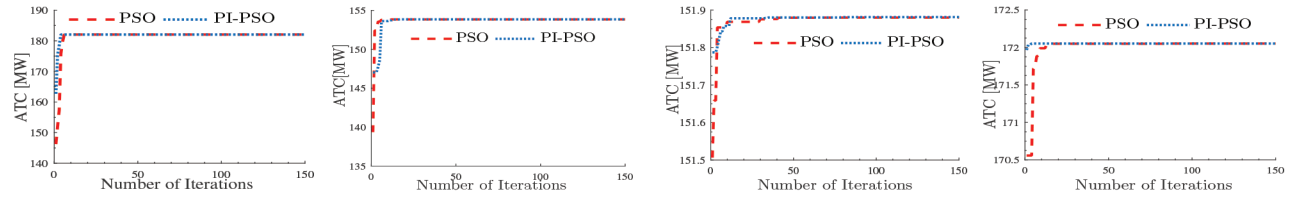


(a) Transaction **T1**. (b) Transaction **T2**. (c) Transaction **T7**. (d) Transaction **T10**.

**Figure 11**. Convergence characteristics for ATC enhancement with TCSC.

Similarly, in Table 4, the effectiveness of PI-PSO regarding superior ATC values compared to PSO is evident in **T1** to **T8** and **T10**. For a typical run of **T2**, **T4**, and **T8**, PSO is trapped in a local optimal location. Likewise, Figure 12 shows the convergence characteristics for a typical run of PSO and PI-PSO with SSSC for **T1** to **T10**. Observe that in Figures 12a–12j, the proposed PI-PSO produces higher ATC compared to PSO and converges in 10–35 iterations. The higher ATC is more pronounced in Figures 12b, 12d, 12f, 12g, and 12h.

**Table 4**. ATC values with SSSC for both PSO and PI-PSO.

| Trans. | ATC [MW] | | | PSO solution | | | PI-PSO solution | | |
|---|---|---|---|---|---|---|---|---|---|
| ID | Base case | PSO | PI-PSO | Line no. | $V_{se}$(p.u.) | $\delta_{se}(^\circ)$ | Line no. | $V_{se}$(p.u.) | $\delta_{se}(^\circ)$ |
| **T1** | 143.2545 | 166.5618 | 166.5841 | 6(8 to 9) | 0.0902 | 158.758 | 6(8 to 9) | 0.08809 | 158.753 |
| **T2** | 127.1567 | 151.2113 | 159.4050 | 8(9 to 6) | 0.0506 | -90.132 | 5(7 to 8) | 0.0999 | 166.301 |
| **T3** | 118.0243 | 142.9949 | 143.0993 | 3(5 to 7) | 0.0473 | -90.863 | 3(5 to 7) | 0.05184 | -76.74 |
| **T4** | 155.1414 | 174.5975 | 176.0799 | 6(8 to 9) | 0.0999 | -116.15 | 8(9 to 6) | 0.05865 | 61.8147 |
| **T5** | 43.6314 | 64.8313 | 64.8441 | 3(5 to 7) | 0.0536 | 54.3691 | 3(5 to 7) | 0.05505 | 43.9809 |
| **T6** | 128.0228 | 163.4792 | 163.8505 | 5(7 to 8) | 0.0279 | 76.0599 | 5(7 to 8) | 0.08479 | 121.235 |
| **T7** | 138.6407 | 153.2279 | 158.5469 | 3(5 to 7) | 0.0616 | -61.091 | 3(5 to 7) | 0.0999 | -35.798 |
| **T8** | 74.6104 | 89.3067 | 89.8998 | 3(5 to 7) | 0.0945 | -49.489 | 2(4 to 5) | 0.07184 | 142.65 |
| **T9** | 60.2851 | 88.3222 | 88.3222 | 5(7 to 8) | 0.0999 | 172.529 | 5(7 to 8) | 0.0999 | 172.536 |
| **T10** | 159.4606 | 169.8679 | 169.9509 | 2(4 to 5) | 0.0594 | 75.6183 | 2(4 to 5) | 0.05654 | 73.5604 |

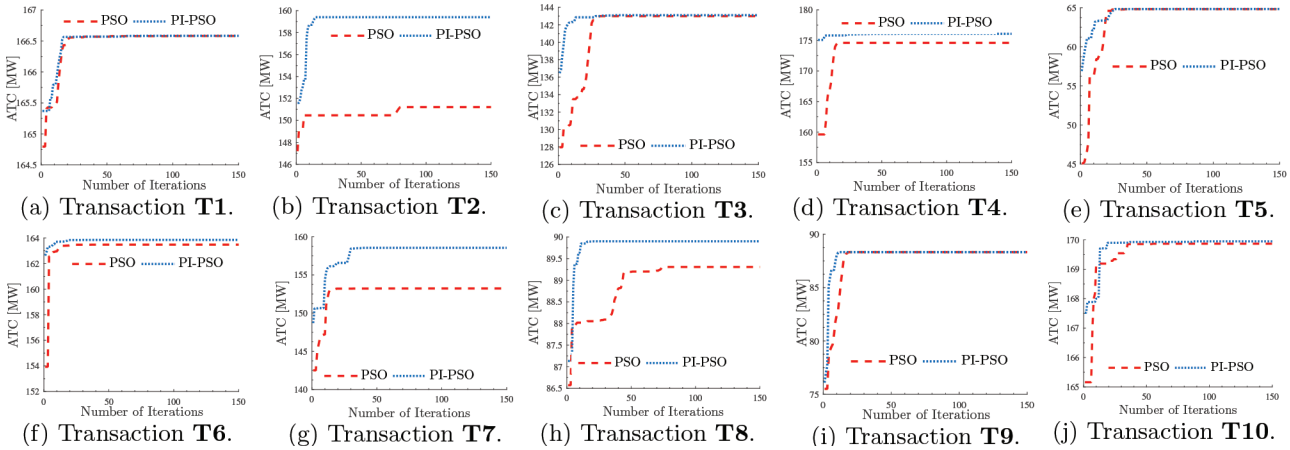


(a) Transaction **T1**. (b) Transaction **T2**. (c) Transaction **T3**. (d) Transaction **T4**. (e) Transaction **T5**.

(f) Transaction **T6**. (g) Transaction **T7**. (h) Transaction **T8**. (i) Transaction **T9**. (j) Transaction **T10**.

**Figure 12**. Convergence characteristics for ATC enhancement with SSSC.

The low number of iterations and higher ATC values translate to superior speed and accuracy of the proposed PI-PSO over PSO. Moreover, the starting point improvement of PI-PSO over PSO is similar to that in Figure 11 with TCSC. These improvements are attributable to better exploration abilities of PI-PSO within the RSS. Furthermore, Figure 13 depicts the plots of particles' positions against $V_{se}$ using PSO and PI-PSO. It is observed that in PI-PSO, all particles converged to the optimal location, with improved exploitation ability of PI-PSO to obtain a superior ATC over PSO.

Average convergence time is measured as the elapse for each particle to reach the optimal location [49]. In Figure 14, the average time with PI-PSO is within 25-–130 s against over 200 s for PSO.

ATC enhancements impact the receiving end voltage profile, which is a key power quality index. Consequently, Figure 15 depicts voltage profile. The base case ATC for **T1** to **T10** and with TCSC for **T3**, **T6**, and **T8** were constrained by Eq. (32). As depicted in Figures 15a–15f, for bus voltages for the case of no FACTS and TCSC, particularly in Figures 15b, 15d, and 15e, they are above minimum (0.9 p.u.). Conversely, ATC with SSSC is constrained by voltage at bus 5 for **T1**; bus 6 for **T3**, **T4**, **T8**, and **T10**; and bus 8 for **T6**. These buses constitute the sink buses.

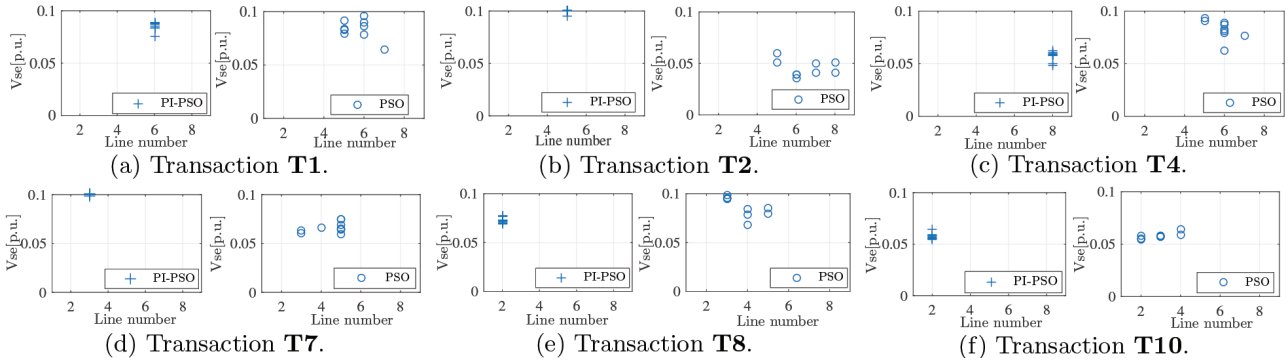


**Figure 13**. Plot of particles' positions versus Vse for PI-PSO and PSO.

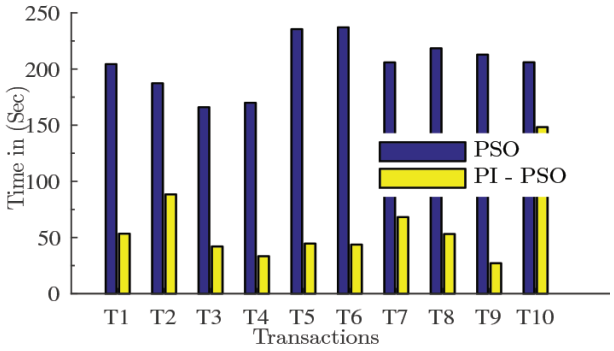


**Figure 14**. Average convergence time for ATC enhancement with SSSC.

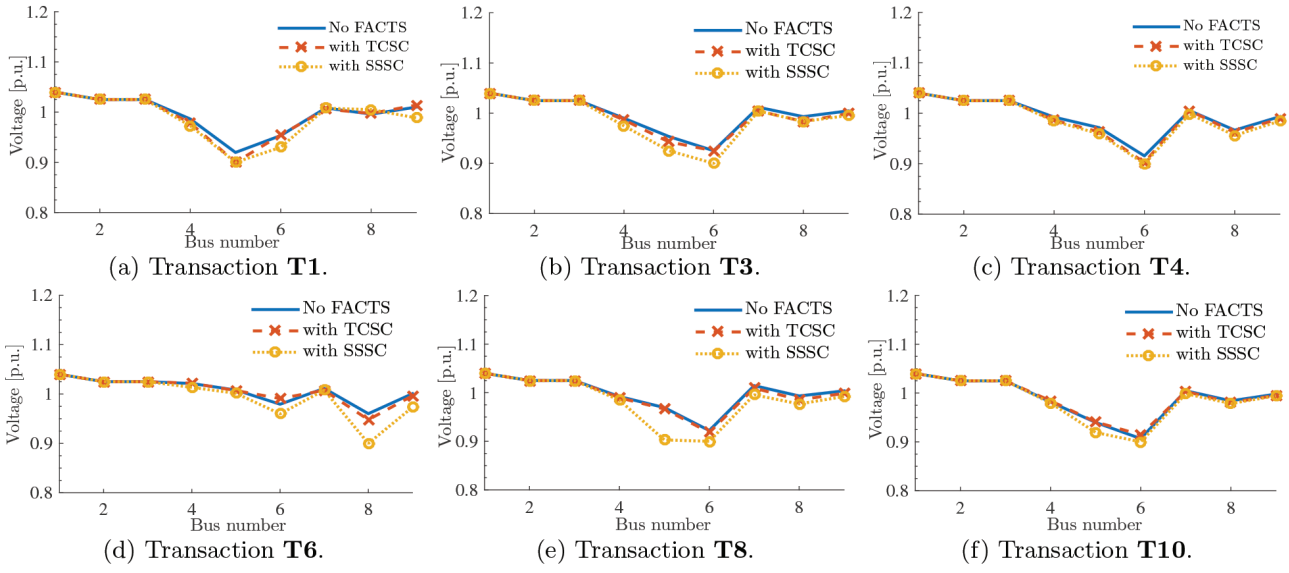


**Figure 15**. Voltage profile of some transactions without and with FACTS.

## 8. Conclusion

A hybrid PI-PSO has been proposed for optimal planning of FACTS to enhance ATC. Sensitivity is used to reduce location search space. Two masking effect reduction methods, iterative n-exponent and Newton's divided difference, were introduced for transactions whose $\partial PI_2$ are characterized by masking effect. The proposed PI-PSO with similar parameters performs better than PSO regarding convergence characteristics and efficiency in obtaining higher ATC values while avoiding the local optima. The performance of PI-PSO is noticeable in VSC-based FACTS with complex optimization variables. In addition, the new features of CPF that ensure ATC computation with respect to line and voltage constraints have been acknowledge by the MATPOWER community.

## Acknowledgment

We would like to acknowledge Shrirang Abhyankar and Ray Zimmerman for code cleaning and test runs of contribution to MATPOWER. CPF options are documented in MATPOWER-Release-Notes-7.0.

## References

[1] Kumar A, Kumar J. ATC with ZIP load model - A comprehensive evaluation with third generation FACTS in restructured electricity markets. International Journal of Electrical Power and Energy Systems 2014; 54 (1): 546–558. doi: 10.1016/j.ijepes.2013.08.003

[2] Alekhaya B, Srinivasa Rao J. Enhancement of ATC in a deregulated power system by optimal location of multi-FACTS devices. In: IEEE 2014 International Conference on Smart Electric Grid; Guntur, India; 2014. pp. 1–9. doi: 10.1109/ISEG.2014.7005599

[3] Anupriya S, Janamala V. Available transfer capability (ATC) enhancement and optimization of UPFC shunt converter location with GSF in deregulated power system. In: IEEE 2016 Intertional Conference on Circuit, Power Computing Technology; Nagercoil, India; 2016. pp. 1-5. doi: 10.1109/ICCPCT.2016.7530289

[4] Khandani F, Soleymani S, Mozafari B. Optimal allocation of SVC to enhance total transfer capability using hybrid genetics algorithm and sequential quadratic programming. In: IEEE 8th International Conference on Electrical Engineering/Electronics, Computer, Telecommunications and Information Technology (ECTI-CON, Association of Thailand - Conference 2011); Khon Kaen, Thailand; 2011. pp. 861–864. doi: 10.1109/ECTICON.2011.5947976

[5] Sinha N, Karan S, Singh SK. Modified DE based ATC enhancement using FACTS devices. In: 1st IEEE International Conference on Computational Intelligence & Networks; Bhubaneshwar, India; 2015. pp. 3–8.

[6] Nireekshana T, Kesava GR, Sivanaga SR. Enhancement of ATC with FACTS devices using real-code genetic algorithm. International Journal of Electrical Power and Energy Systems 2012; 43 (1): 1276–1284. doi: 10.1016/j.ijepes.2012.06.041

[7] Choudhury NB, Jena R. Available transfer capability enhancement in constrained network conditions using TCSC. In: IEEE 2014 International Conference on Advances in Engineering & Technology Research; Unnao, India; 2014. pp. 1–7. doi: 10.1109/ICAETR.2014.7012804

[8] Balasubbareddy M, Sivanagaraju S, Venkata C. A non-dominated sorting hybrid cuckoo search algorithm for multi-objective optimization in the presence of FACTS devices. Russian Electrical Engineering 2017; 88 (1): 44–53. doi: 10.3103/S1068371217010059

[9] Esmaeili A, Esmaeili S. A new multiobjective optimal allocation of multitype FACTS devices for total transfer capability enhancement and improving line congestion using the harmony search algorithm. Turkish Journal Electrical Engineering & Computer Science 2013; 21 (4): 957–979. doi: 10.3906/elk-1108-66

[10] Glazunova AM, Aksaeva ES, Semshchikov ES. Forecasting of available transfer capability in inter-system transmission lines. In: 2016 IEEE International Energy Conference; Leuven, Belgium; 2016. pp. 1–6.

[11] Sadiq AA, Nwohu MN, Okenna AE. Available transfer capability as index for transmission network performance: a case study of nigerian 330 kV transmission grid. International Journal Electrical Engineering and Informatics 2014; 6 (3): 479–496.

[12] Nireekshana T, Kesava GR, Sivanaga SR. Available transfer capability enhancement with FACTS using cat swarm optimization. Ain Shams Engineering Journal 2016; 7 (1): 159–167. doi: 10.1016/j.asej.2015.11.011

[13] Sharma S, Vadhera S. Enhancement of power transfer capability of interconnected power system using unified power flow controller (UPFC). International Journal of Electronics and Electrical Engineering 2016; 4 (3): 5–10. doi:10.18178/ijeee.4.3.199-202

[14] Kamel S, Jurado F, Peças Lopes JA. Comparison of various UPFC models for power flow control. Electric Power Systems Research 2015; 121 (1): 243–251. doi: 10.1016/j.epsr.2014.11.001

[15] Venkateswara RM, Sivanagaraju S, Suresh CV. Available transfer capability evaluation and enhancement using various FACTS controllers: special focus on system security. Ain Shams Engineering Journal 2016; 7 (1): 191–207. doi: 10.1016/j.asej.2015.11.006

[16] Khafafi K, Sakhavati A, Nahi S. Optimal locating and sizing of SSSC using genetic algorithm in deregulated power market. International Journal of Computer Applications 2011; 22 (4): 37–41.

[17] Nimje AA, Panigrahi CK, Mohanty AK. Enhanced power transfer capability by using SSSC. Journal of Mechanical Engineering Research 2011; 3 (2): 48–56.

[18] Kumar A, Jitender K. ATC enhancement in electricity markets with GUPFC and IPFC - a comparison. Electrical Power and Energy Systems 2016; 81 (1): 469–482. doi: 10.1016/j.ijepes.2016.02.047

[19] Kumar KS, Basavaraja B, Sanker Ram, BV. Optimal placement of FACTS devices with available transfer capability enhancement. In: 2014 International Conference on Smart Electric Grid; Guntur, India; 2014. pp. 1–4. doi: 10.1109/ISEG.2014.7005597

[20] Bavithra K, Raja SC, Venkatesh P. Optimal setting of FACTS devices using particle swarm optimization for ATC enhancement in deregulated power system. IFAC-PapersOnLine 2016; 49 (1): 450-455. doi: 10.1016/j.ifacol.2016.03.095

[21] Farahmand H, Rashidinejad M, Mousavi A, Gharaveisi AA, Irving MR et al. Hybrid mutation particle swarm optimisation method for available transfer capability enhancement. International Journal of Electrical Power and Energy Systems 2012; 42 (1): 240–249. doi: 10.1016/j.ijepes.2012.04.020

[22] Ngatchou P, Zarei A, El-Sharkawi MA. Pareto multi-objective optimization. In: 13th International Conference on Intelligent Systems Application to Power Systems; Arlington, VA, USA; 2005. pp. 84–91. doi: 10.1109/ISAP.2005.1599245

[23] Manganuri Y, Choudekar P, Abhishek, Asija D, Ruchira. Optimal location of TCSC using sensitivity and stability indices for reduction in losses and improving the voltage profile. In: 2016 IEEE 1st International Conference on Power Electronics, Intelligent Control and Energy Systems; Delhi, India; 2016. pp. 1–4.

[24] Arulraj R, Kumarappan N. Optimal economic-driven planning of multiple DG and capacitor in distribution network considering different compensation coefficients in feeder's failure rate evaluation. Engineering Science and Technology an International Journal 2019; 22 (1): 67-77. doi: 10.1016/j.jestch.2018.08.009

[25] Kavitha K, Neela R. Comparison of BBO, WIPSO & PSO techniques for the optimal placement of FACTS devices to enhance system security. Procedia Technology, 2016; 25: 824–837. doi: 10.1016/j.protcy.2016.08.186

[26] Dobson I, Greene S, Rajaraman R, DeMarco CL, Alvarado FL et al. Electric power transfer capability: concepts, applications, sensitivity and uncertainty. Ithaca, NY, USA: Cornell University, 2001.

[27] Bone G, Mihalič R. Modelling the SSSC device in the power flow problem as power injections regulated according to first order sensitivity. Engineering and Industry Series, Deregulated Electricity Market Issues in South Eastern Europe 2015; 2015: 80–85. doi: 10.22618/TP.EI.20151.192013

[28] Kamel S, Jurado F. Fast decoupled load flow analysis with SSSC power injection model. IEEJ Transactions on Electrical and Electronic Engineering 2014; 9 (4): 370–374. doi: 10.1002/tee.21981

[29] Varshini GYS, Kalpana N. Enhancement of available transfer capability using particle swarm optimization technique with interline power flow controller. In: Third International Conference on Sustainable Energy and Intelligent Systems; Tamil Nadu, India; 2012. pp. 331–334. doi: 10.1049/cp.2012.2234

[30] Kumar A, Kumar J. Comparison of UPFC and SEN transformer for ATC enhancement in restructured electricity markets. Electrical Power and Energy Systems 2012; 41 (1): 96–104. doi: 10.1016/j.ijepes.2012.03.019

[31] Prathiba R, Balasinghs M, Devaraj D, Karuppasamypandiyan M. Multiple output radial basis function neural network with reduced input features for on-line estimation of available transfer capability. Control Engineering and Applied Informatics 2016; 18 (1): 95–106.

[32] Idris RM, Kharuddin A, Mustafa MW. Optimal allocation of FACTS devices for atc enhancement using bees algorithm. In: Power Engineering Conference; Adelaide, Australia; 2009. pp. 318–325.

[33] Chansareewittaya S, Jirapong P. Power transfer capability enhancement with multi-type FACTS controllers using particle swarm optimization. In: IEEE 11th International Conference on Electrical Engineering/Electronics, Computer, Telecomms and IT; Nakhon Ratchasima, Thailand; 2014. pp. 1–6. doi: 10.1109/TENCON.2010.5685893

[34] Babulal CK, Kannan PS. A novel approach for ATC computation in deregulated environment. Journal of Electrical Systems 2006; 2 (3): 146–161.

[35] Khosravifard M, Shaaban M. Risk-based available transfer capability assessment including non-dispatchable wind generation. International Transactions on Electrical Energy Systems 2015; 25 (11): 3169–3183. doi: 10.1002/etep.2036

[36] Dou X, Zhang S, Chang L, Wu Z, Gu W et al. An improved CPF for static stability analysis of distribution systems with high DG penetration. Electrical Power and Energy Systems 2017; 86 (3): 177-188.

[37] Prathiba R, Moses MB, Karuppasamypandiyan M. Optimal selection and allocation of generator for static ATC using differential evolution algorithm. International Journal of Engineering and Technology 2014; 6 (2): 948–959.

[38] Canizares CA, Berizzi A, Marannino P. Using FACTS controllers to maximize available transfer capability. In: Proceedings of the Bulk Power Systems Dynamics and Control IV—Restructuring; Santorini, Greece; 1998. pp. 633–641.

[39] Lubis RS, Hadi SP. Selection of suitable location of the FACTS devices for optimal power flow. International Journal of Electrical & Computer Sciences 2012; 12 (3): 38–49.

[40] Srinivasa Rao V, Srinivasa Rao R. Comparison of various methods for optimal placement of FACTS devices. In: 2014 International Conference on Smart Electric Grid; Guntur, India; 2014. pp. 1–7.

[41] Manikandan S, Arul P. Optimal location of multiple FACTS device using sensitivity methods. International Journal of Engineering Trends and Technology 2013; 4 (10): 4361–4367.

[42] Eghtedarpour N, Seifi AR, Sensitivity-based method for the effective location of SSSC. Journal of Power Electronics 2011; 11 (1): 90–96. doi: 10.6113/JPE.2011.11.1.090

[43] Srinivasa Rao R, Srinivasa Rao V. A generalized approach for determination of optimal location and performance analysis of FACTS devices. Electrical Power and Energy Systems 2015; 73 (1): 711–724. doi: 10.1016/j.ijepes.2015.06.004

[44] Schbfer KF, Verstege JF. Adaptive procedure for masking Effect compensation in contingency selection algorithm. IEEE Transactions on Power Systems 1990; 5 (2): 539–546.

[45] Vemuri S, Usher RE. On-line automatic contingency selection algorithms. IEEE Transactions on Power Apparatus and Systems 1983; 102 (2): 346–354. doi: 10.1109/MPER.1983.5519626

[46] Dahal S, Salehfar H. Impact of distributed generators in the power loss and voltage profile of three phase unbalanced distribution network. Electrical Power and Energy Systems 2016; 77 (1): 256–262. doi: 10.1016/j.ijepes.2015.11.038

[47] Sadiq AA, Adamu SS, Buhari M. Optimal distributed generation planning in distribution networks: a comparison of transmission network models with FACTS. Engineering Science and Technology - An International Journal 2019; 22 (1): 33-46. doi: 10.1016/j.jestch.2018.09.013

[48] Zimmerman RD, Murillo-Sanchez CE, Thomas RJ. MATPOWER: steady-state operations, planning, and analysis tools for power systems research and education. IEEE Transaction on Power Systems 2011; 26 (1): 12–19. doi: 10.1109/TPWRS.2010.2051168

[49] Gupta A, Kumar A. ATC determination with heuristic techniques and comparison with sensitivity based methods and GAMS. Procedia Computer Science 2018; 125 (1): 389–397. doi: 10.1016/j.procs.2017.12.051